Peer-reviewed version available at Polymers 2019, 11, 131; doi:10.3390/polym11010131

Article

Synchronized Molecular-Dynamics Simulation of the Thermal Lubrication of an Entangled Polymeric Liquid

Shugo Yasuda[1,*]

[1] Graduate School of Simulation Studies, University of Hyogo, Kobe 650-0047, Japan; yasuda@sim.u-hyogo.ac.jp

* Correspondence: yasuda@sim.u-hyogo.ac.jp

Abstract: The thermal lubrication of an entangled polymeric liquid in wall-driven shear flows between parallel plates is investigated by using a multiscale hybrid method coupling molecular dynamics and the hydrodynamics (i.e., the synchronized molecular dynamics method). The temperature of the polymeric liquid rapidly increases due to viscous heating once the drive force exceeds a certain threshold value. The rheological properties of the polymeric liquid drastically change at around the critical drive force. In the weak viscous-heating regime, the conformation of polymer chains is dominated by the local shear flow so that the anisotropy of the bond orientation tensor grows as the drive force increases. However, in the large viscous-heating regime, the conformation dynamics is dominated by the thermal agitation of polymer chains so that the bond orientation tensor recovers more uniform and random structures as the drive force increases, even though the local shear flows are further enhanced. Remarkably, these counter-intuitive transitional behaviors give an interesting re-entrant transition in the stress–optical relation, where a linear formalism in the stress–optical relation approximately holds even though each of the macroscopic quantities behaves nonlinearly. The robustness of the linear stress–optical relation is also confirmed in the spatiotemporal evolution at the hydrodynamic level.

Keywords: multiscale modeling; polymeric liquid; entanglement; viscous heating; lubrication

1. Introduction

Polymeric fluids exhibit complicated flow behaviors because the microscopic dynamics of polymer chains are highly correlated with the global hydrodynamic transport. [1]. Especially, in high-speed devices, the microscopic dynamics are significantly affected by viscous heating because the polymeric fluid has a large Prandtl number, so the microscopic dynamics and the hydrodynamic heat and momentum transports are mutually correlated. Predicting the microscopic dynamics and the macroscopic thermal flows in high-speed devices is challenging from both scientific and engineering points of view. Computer simulations are expected to be useful to solve these mutually-correlated multiscale systems.

Multiscale simulations to tackle the flow behaviors of complex fluids have been developed by various researchers. The CONNFFESSIT approach was first proposed for polymeric liquids by Laso and Öttinger [2–4], where the local stress in the fluid solver is calculated by a microscopic simulation without using any constitutive relations. The strategy exploited in the CONNFFESSIT approach is also introduced into heterogeneous multiscale modeling (HMM), which was proposed by E and Enquist [6]. HMM has been applied to various problems [7–9]. The equation-free multiscale computation proposed by Kevrekids et al. is based on a similar idea, and has been applied to various problems [10,11]. De et al. proposed the scale-bridging method, which succeeded in reproducing the memory effect of a polymeric liquid correctly and demonstrated the nonlinear viscoelastic behavior of a polymeric liquid in slab and cylindrical geometries [12,13]. The multiscale simulation of polymeric flows with

the advection of memory in two and three dimensions was developed by Murashima and Taniguchi [14–16]. Noise reduction algorithms in filtering the microscopic particle-based simulation data in hybrid multiscale moedling were also investigated in Ref. [17].

We have also developed multiscale simulations which couple the molecular dynamics and hydrodynamic transports. The method was first developed for a simple Lennard-Jones fluid [18] and subsequently extended to polymeric liquids with the memory effect [19–22]. Recently, we proposed the synchronized molecular dynamics (SMD) method for thermal lubrication flows of polymeric liquids, in which the local viscous heating is autonomously generated in the local MD cell according to the local shear flow. The local MD cells are also synchronized to satisfy the global heat and momentum transports [23–25].

In this paper, we tackle the thermal lubrication of entangled polymer chains by using the SMD method (we only considered short polymer chains in the previous studies). The spatio-temporal dynamics of entangled polymer chains in local fluid elements under high-speed lubrications is investigated in detail. In the following, we first describe the problem and the model polymeric liquid considered in this paper. Here we also clarify the intrinsic properties in the relaxation dynamics of the entangled polymer chains in comparison to those described by the reptation theory [26]. The SMD method is described in Section 3 and the results and their discussion are given in Section 4. Finally we give a brief summary.

2. Problem

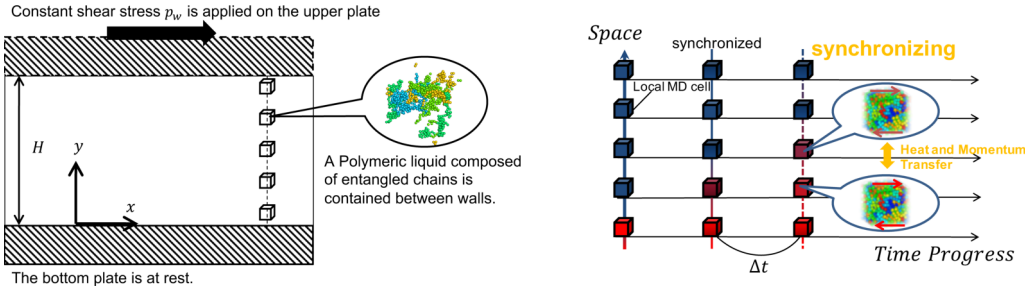

(a) Geometry of problem (b) Time marching scheme

Figure 1. Schematics of (**a**) the geometry of the problem and (**b**) the time marching scheme of synchronized molecular dynamics simulation.

2.1. Geometry

We consider a polymeric liquid confined between parallel walls, as in Figure 1. The upper wall starts to move in the x-direction at time $t = 0$ by an applied shear stress p_w, while the temperature of the walls T_w is kept constant.

The polymeric liquid is initially in a quiescent state with uniform density ρ_0 and temperature T_0, where the initial temperature of the polymeric liquid is the same as the wall temperature (i.e., $T_0 = T_w$).

The polymeric liquid starts to deform the quiescent state at $t = 0$ and forms non-uniform distributions of velocity and temperature via the heat and momentum transfers described by

$$\rho_0 \frac{\partial v_x}{\partial t} = \frac{\partial p_{xy}}{\partial y}, \tag{1a}$$

$$\rho_0 \frac{\partial e}{\partial t} = p_{xy}\dot{\gamma} + \lambda \frac{\partial^2 T}{\partial y^2}, \tag{1b}$$

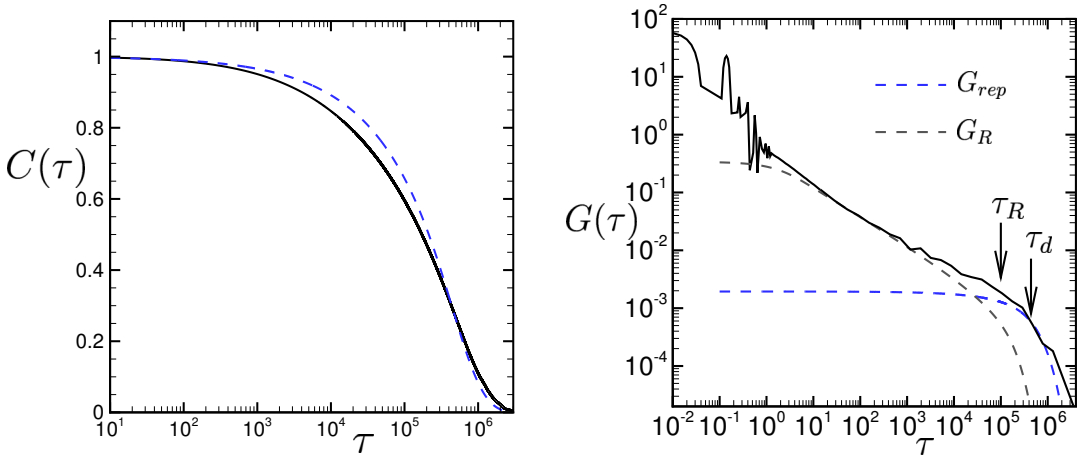

(a) (b)

Figure 2. (**a**) The time-correlation function of the end-to-end vector of polymer chain $C(t)$ defined in Equation (4) and (**b**) the stress relaxation function $G(t)$ defined in Equation (5). In (a), the blue dashed line shows the theoretical formalism of the reptation dynamics with the relaxation time $t_d = 4.4 \times 10^5$. In (b), the theoretical formalisms of the stress relaxation function for the Rouse dynamics, $G_R(t)$ in Equation (7), and for the reptation dynamics, $G_{rep}(t)$ in Equation (8), are also plotted.

where v_α is the velocity, $p_{\alpha\beta}$ is the stress tensor, e is the internal energy per unit mass, and $\dot{\gamma}$ is the shear rate (i.e., $\dot{\gamma} = \partial v_x/\partial y$). Hereafter, the subscripts α, β, and γ represent the index of Cartesian coordinates (i.e., $\{\alpha, \beta, \gamma\} \in \{x, y, z\}$). Here, we assum that the macroscopic quantities are uniform in the x and z directions, $\partial/\partial x = \partial/\partial z = 0$, and the density of the polymeric liquid is constant. Fourier's law for heat flux with a constant and uniform thermal conductivity λ is also considered in Equation (1b).

We also consider the non-slip and non-jump boundary conditions of velocity and temperature for Equation (1). That is, the velocity and temperature of the polymeric liquid on the wall are the same as those of the wall.

2.2. Model Polymeric Liquid

The polymeric liquid is composed of so-called Kremer–Grest chains of 250 beads, where each bead particle interacts via the repulsive part of the Lennard-Jones potential,

$$U_{\mathrm{LJ}}(r) = \begin{cases} 4\epsilon\left[\left(\frac{\sigma}{r}\right)^{12} - \left(\frac{\sigma}{r}\right)^{6}\right] + \epsilon, & (r \le 2^{1/6}\sigma), \\ 0, & (r \ge 2^{1/6}\sigma), \end{cases} \tag{2}$$

and consecutive beads on each chain are connected by an anharmonic spring potential,

$$U_{\mathrm{F}}(r) = -\frac{1}{2}k_c R_0^2 \ln\left[1 - \left(\frac{r}{R_0}\right)^2\right], \tag{3}$$

with $k_c = 30\epsilon/\sigma^2$ and $R_0 = 1.5\sigma$ [27]. Hereafter, unless otherwise stated, we measure the physical quantities with the units of length σ, time $\sqrt{m\sigma^2/\epsilon}$, and temperature ϵ/k_B, where m is the mass of the bead particle and k_B is Boltzmann's constant.

In this study, we only consider a polymeric liquid with the initial density $\rho_0 = 0.85$ and initial temperature $T_0 = 0.4$. Note that the wall temperature $T_w = 0.4$ and the number of beads in each polymer chain $N_b = 250$ are fixed. With this bead number $N_b = 250$, the model polymeric liquid shows the characteristic behaviors of entangled polymer chains in the relaxation dynamics.

Figure 2 shows the normalized time-correlation function of the end-to-end vector of polymer chain $C(\tau)$, which is calculated as

$$C(\tau) = \frac{\left\langle \overline{\mathbf{P}(\tau + t_0) \cdot \mathbf{P}(t_0)} \right\rangle}{\left\langle \overline{|\mathbf{P}(t_0)|^2} \right\rangle}, \tag{4}$$

and the stress relaxation function $G(\tau)$, which is calculated as

$$G(\tau) = \frac{T_0}{V} \overline{p_{xy}(\tau + t_0) p_{xy}(t_0)} \tag{5}$$

for the present model polymeric liquid. Here, $\mathbf{P}(\mathbf{t})$ represents end-to-end vectors of each polymer chain, $p_{xy}(t)$ is the macroscopic shear stress, which is the average of the microscopic shear stresses of each bead particle in the simulation box, and V is the volume of the simulation box. We also write $\overline{X(t_0)}$ as the average of X with respect to t_0 and $\langle X \rangle$ as the ensemble average of X over all chains.

In Figure 2a , our numerical result of $C(t)$ is compared with a theoretical formalism, which is obtained in both the Rouse dynamics and the reptation dynamics,

$$C_r(\tau) = \sum_{\text{odd}\, p} \frac{8}{\pi^2 p^2} \exp(-p^2 \tau / \tau_d), \tag{6}$$

where the summation is over odd p and $1 \leq p \leq N_b - 1$.[26]

The relaxation time $\tau_d = 4.4 \times 10^5$ is measured by fitting Equation (6) with our numerical result at $\tau = \tau_d$ (i.e., $C_r(\tau_d) = C(\tau_d)$). We note that the relaxation time τ_d corresponds to the disengagement time τ_d of entangled polymer chains if we assume that the time correlation function is described by the reptation dynamics.

In Figure 2b, the numerical result of the stress relaxation function $G(\tau)$ is compared with the theoretical formalisms for the Rouse dynamics $G_R(\tau)$ and for the reptation dynamics $G_{rep}(\tau)$ which are written, respectively, as

$$G_R(\tau) = \frac{\rho_0 T_0}{N_b} \sum_{p=1}^{N_b - 1} \exp(-p^2 t / \tau_R N_b^2), \tag{7}$$

and

$$G_{rep}(\tau) = \frac{\rho_0 T_0}{N_e} C_r(\tau). \tag{8}$$

Here, the Rouse relaxation time $\tau_R = 1.0 \times 10^5$ and the average number of beads between entanglements $N_e = 175$ are estimated from our numerical results. Numerical results of τ_d and Ne for the Kremer–Grest chains with different parameters can be found in Ref. [29] and the references therein.

The average number of beads between entanglements is measured by fitting the formula Equation (8) with our numerical result at $\tau = \tau_d$. The Rouse relaxation time τ_R is calculated by the formula $\tau_d / \tau_R = 3 N_b / N_e$.

In Figure 2, it can be seen that the relaxation dynamics of the model polymeric liquid is well-described by the reptation dynamics for entangled polymer chains at long times (i.e., $\tau > \tau_r$). The transition of the Rouse dynamics to the reptation dynamics can also be clearly observed in the stress relaxation function.

The viscosity of the model polymeric liquid in the quiescent state $\eta_0 = 980$ is calculated from the stress relaxation function $G(\tau)$ as $\eta_0 = \int_0^{\tau_\infty} G(\tau) d\tau$. The integral with respect to τ is almost saturated at $\tau_\infty = 2 \times 10^6$ and the deviation of η_0 in the period for $\tau_\infty = 2 \times 10^6$ to 5×10^6 is at most 8%.

Preprints (www.preprints.org) | NOT PEER-REVIEWED | Posted: 8 November 2018 doi:10.20944/preprints201811.0223.v1

Peer-reviewed version available at Polymers 2019, 11, 131; doi:10.3390/polym11010131

3. Simulation Method

We investigate the thermal lubrication of the polymeric liquid composed of entangled chains by using the synchronized molecular dynamics (SMD) simulation [23]. In the SMD method, the gap between the upper and lower walls is divided into M mesh intervals with a uniform width of $\Delta y = H/M$, and the local velocities are calculated at each mesh node by using a usual finite volume scheme of Equation (1a). The local shear stresses $p_{xy}(y)$ are calculated in the sub-MD cells associated with each mesh interval according to the local shear rates by using the NEMD simulation with the SLLOD algorithm [30,31]. The MD simulations are performed in a time interval Δt, and the time integrals of the instantaneous shear stresses $\mathcal{P}_{xy}$ in each MD cell are used to update the local velocities at the next time step in accordance with the macroscopic momentum transport Equation (1a),

$$v_x^n(y) = v_x^{n-1}(y) + \frac{\partial}{\partial y}\int_{(n-1)\Delta t}^{n\Delta t} \mathcal{P}_{xy}(\tau;\dot{\gamma}^{n-1}(y))d\tau. \tag{9}$$

Here, the superscript n represents the time step number, $\mathcal{P}_{xy}(\tau;\dot{\gamma}^{n-1}(y))$ is the instantaneous shear stress in the NEMD simulation with the shear rate $\dot{\gamma}^{n-1}(y)$, and τ is the time in the NEMD simulation.

We note that he final configuration obtained for the molecules in each MD cell at each time step $n\Delta t$ is retained as the initial configuration for the MD cell in the next time step $(n+1)\Delta t$. Thus, we trace the complete temporal evolution of the microscopic configurations with a microscopic time step so the memory effects can be reproduced correctly.

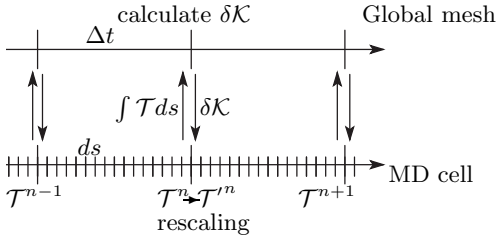

Figure 3. Schematic for the calculation of the temperature in the synchronized molecular dynamics (SMD) method. The upper side represents the progress on the global mesh system, and the lower side represents the progress at each MD cell. The time-step size in the MD cell, ds, is much smaller than that in the global transport Δt.

The local viscous heating caused by shear flow (i.e., the first term of Equation (1b)), is autonomously calculated in the NEMD simulations without using any thermostat algorithms, but at each time interval Δt, the instantaneous kinetic energies of the molecules per unit mass $\mathcal{K}$ in each MD cell are corrected according to the heat fluxes between neighbor MD cells. That is,

$$\delta\mathcal{K} = \frac{\lambda}{\rho_0}\frac{\partial^2}{\partial y^2}\int_{(n-1)\Delta t}^{n\Delta t} \mathcal{T}(s)ds, \tag{10}$$

where $\mathcal{T}$ is the instantaneous temperature of the MD cell and s is the time progress in the MD cell. That is, the molecular velocities in the MD cell are rescaled according to the corrected temperature $\mathcal{T}'$, i.e.,

$$\mathcal{T}' = \mathcal{T} + \frac{2}{3}\delta\mathcal{K}, \tag{11}$$

at each time interval Δt. See also Figure 3.

Thus, the MD simulations assigned to each fluid element are synchronized at time intervals of Δt to satisfy the macroscopic heat and momentum transport equations, as illustrated in Figure 1(b). Note that the temperature rise caused by local viscous heating is calculated autonomously in the MD simulation, and satisfies the macroscopic energy balance of Equation (1b).

4. Results and Discussion

The SMD simulation is performed for the geometry shown in Figure 1. At time $t = 0$, the shear stress p_w is applied on the upper wall and the upper wall starts to move in the x direction. The upper wall drives the polymeric liquid, and spatial profiles of the velocity $v_x(y)$, temperature $T(y)$, and polymer conformation (i.e., the bond-orientation tensor) $Q_{\alpha\beta}(y)$ are created between the walls.

The local bond-orientation tensors $Q_{\alpha\beta}(y)$ are calculated in each MD cell as

$$Q_{\alpha\beta} = \frac{1}{N_p} \sum_{\text{chains}} \frac{1}{N_b - 1} \sum_{j=1}^{N_b - 1} \frac{b_{j\alpha}}{b_{\min}} \frac{b_{j\beta}}{b_{\min}}, \tag{12}$$

where N_p is the number of polymer chains in each MD cell, $\boldsymbol{b}_j$ for $1 \le j \le N_b - 1$ is the bond vector between consecutive beads in the same chain, and $b_{\min}$ is the distance at which the sum $U_{\text{LJ}}(r) + U_F(r)$ has a minimum (i.e., $b_{\min} \simeq 0.97$).

The initial density and temperature, $\rho_0 = 0.85$ and $T_0 = 0.4$, the wall temperature $T_w = 0.4$, and the channel width $H = 5000$ are fixed while the drive force on the upper wall is varied as $p_w = 0.0005$, 0.001. 0.002. 0.005, 0.01, 0.02, 0.03, 0.05, 0.07, and 0.09.

In the numerical scheme, the number of mesh intervals $M = 32$, that is, $\Delta y = 156.25$, the time interval in Equation (9) $\Delta t = 1$, the time-step size of MD simulation $\Delta t_{\text{MD}} = 0.0025$, and the number of polymer chains in each MD cell $N_p = 32$ are also fixed. Thus, $N_b \times N_p = 8000$ bead particles are included in each MD cell with the side length $l_{MD} = 21$. We also fix the thermal conductivity in Equation (10) as $\lambda/\rho_0 = 100$.

4.1. Spatial Distribution

Figure 4 shows the spatial distribution of the velocity, temperature, shear stress, and bond orientation in the stationary state. The local quantities are time-averaged over $t = [1 \times 10^6, 1.5 \times 10^6]$ for $p_w < 0.01$ and $t = [1.3 \times 10^6, 1.5 \times 10^6]$ for $p_w \ge 0.01$.

It can be seen that the local shear stresses are spatially uniform and coincid with the drive forces p_w on the upper wall. This confirms that the momentum transport is balanced so that the macroscopic quantities are in the stationary state.

For small drive forces (i.e., $p_w \le 0.01$), the temperature and bond orientation are almost uniform and the velocity is linear. On the contrary, for large drive forces (i.e., $p_w \ge 0.03$), the spatial variations of the temperature and bond orientation become remarkable and the velocity profile becomes S-shaped. This velocity profile indicates that shear thinning occurrs near the walls.

The temperature rise in the middle of the channel due to viscous heating, and this affects the local polymer conformation in the bond orientation. Interestingly, the local bond orientation Q_{xy} monotonically increases as the drive force p_w in the vicinities of walls while, in the middle of the channel, it behaves non-monotonically against the drive force. This nonlinear behavior is related to the viscous heating.

4.2. Gross Rheological Properties

In this subsection we consider the gross rheological properties of the lubrication system (i.e., the apparent viscosity $\bar{\eta}$), which can be measured from the upper-wall velocity and drive force, the spatial average of the temperature $\bar{T}$, and the spatial average of the bond orientation $\bar{Q}_{\alpha\beta}$.

We define the gross shear rate $\dot{\Gamma}$ by $\dot{\Gamma} = v_w/H$, where v_w is the upper-wall velocity. Because we consider the non-slip boundary condition, the upper-wall velocity is obtained from the velocity of polymeric liquid at $y = H$ (i.e., $v_w = v_x(y = H)$). Then, the apparent viscosity is calculated as $\bar{\eta} = p_w/\dot{\Gamma}$.

Figure 5 shows the apparent viscosity $\bar{\eta}$ and the spatial averages of temperature $\bar{T}$ and bond orientation of polymer chains $\bar{Q}_{\alpha\beta}$. The apparent viscosity approaches the intrinsic viscosity η_0 in

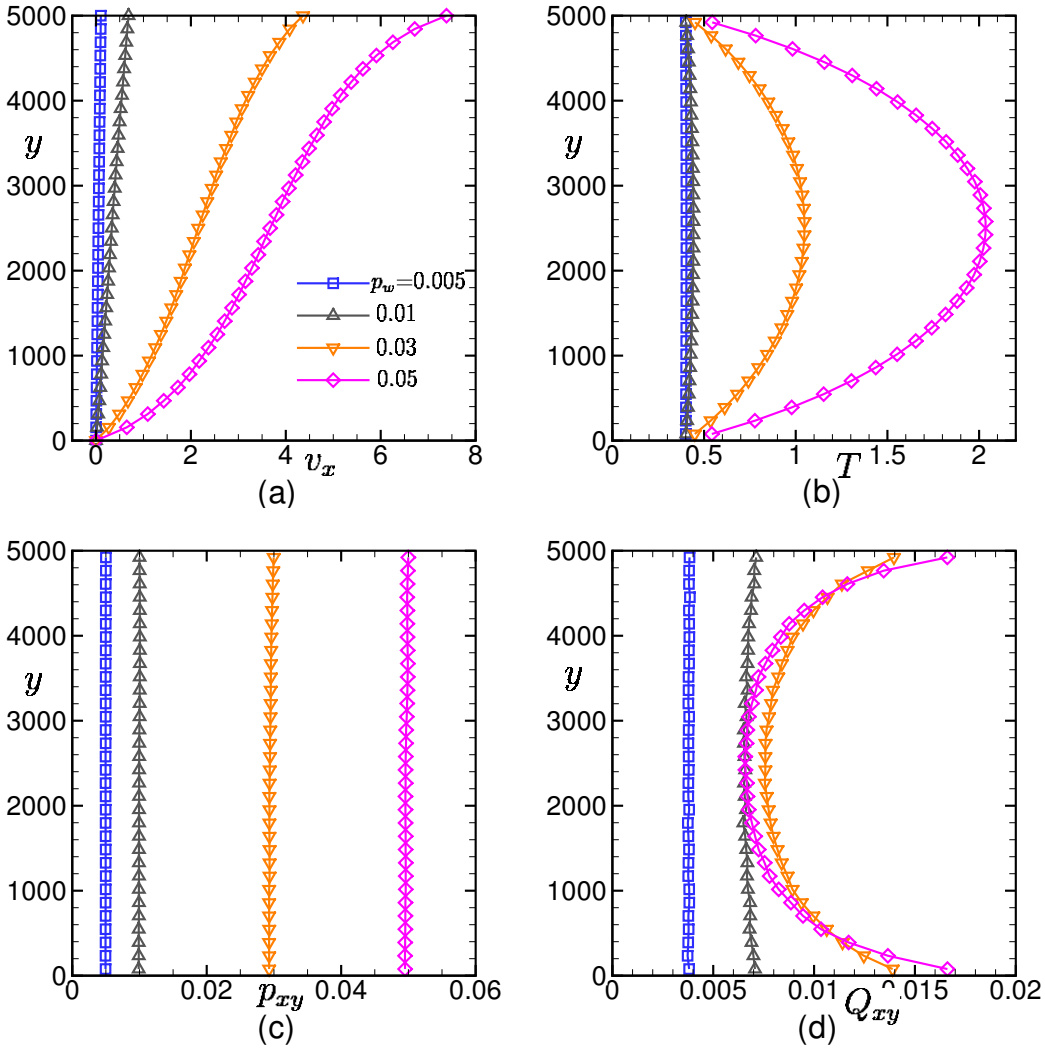

Figure 4. Spatial distributions of the (**a**) velocity, (**b**) temperature, (**c**) shear stress, and (**d**) bond orientation in the stationary state. The results for the different drive forces p_w = 0.005, 0.01, 0.03, and 0.05 are shown.

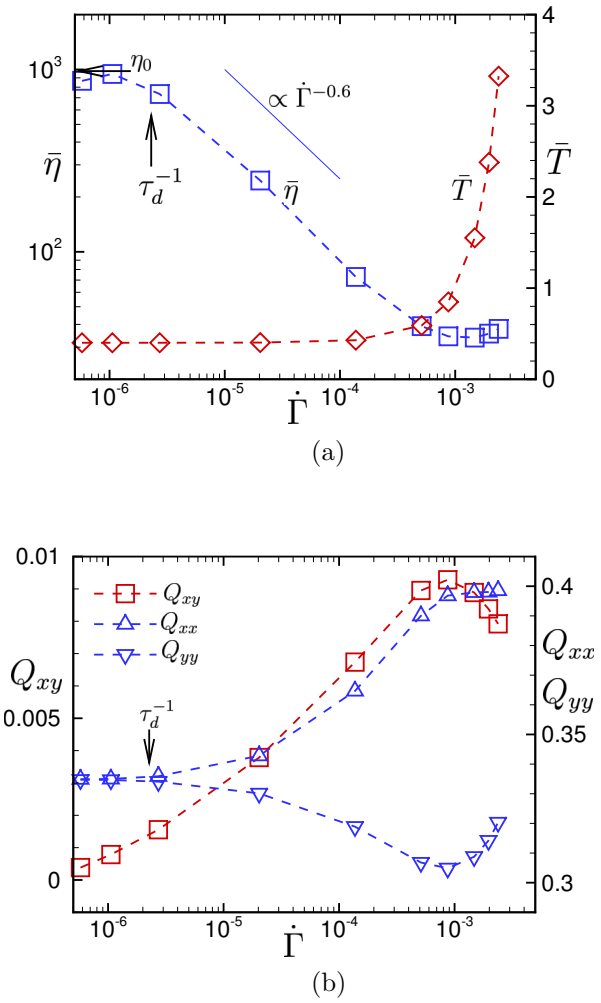

Figure 5. (**a**) The apparent viscosity $\bar{\eta}$ and the spatial average of the local temperature $\bar{T}$ against the gross shear rate $\dot{\Gamma}$, which is defined by the ratio of the upper-wall velocity v_w to the channel width H, $\dot{\Gamma} = v_w/H$. (**b**) The spatial average of the local bond-orientation tensor $\bar{Q}_{\alpha\beta}$ against the gross shear rate $\dot{\Gamma}$. The viscosity of the model polymeric liquid in the quiescent state η_0 is also shown in (a). The rate of disengagement of entangled polymer chains in the reptation dynamics τ_d^{-1} are also shown in (a) and (b).

the quiescent state as the gross shear rate $\dot{\Gamma}$ decreases. When the gross shear rate exceeds the inverse of the disengagement time of the entangled polymer chains (i.e., $\dot{\Gamma} > \tau_d^{-1}$), shear thinning behavior is observed, where the index of the power-law approximation is -0.6. However, the shear thinning behavior ends at $\dot{\Gamma} \simeq 5 \times 10^{-4}$ and, unexpectedly, even a weak shear thickening behavior is observed for $\dot{\Gamma} > 10^{-3}$. The weak shear thickening behavior is obviously related to the rapid temperature rise due to the viscous heating in the large $\dot{\Gamma}$ regime. We note that the shear thickening behavior was not observed in the previous study for the super-cooled polymeric liquid composed of short chains, where the shear thinning behavior is even enhanced when the rapid temperature rise due to the viscous heating occurs.

The transitional behavior triggered by the viscous heating is also observed in the bond orientation of polymer chains. It can be seen from the bond-orientation tensor that polymer chains are stretched in the x direction, and the xy component of the bond-orientation tensor linearly increases as the gross shear rate when the gross shear rate is in the regime $\dot{\Gamma} \lesssim 5 \times 10^{-4}$. However, when $\dot{\Gamma} > 10^{-3}$, the anisotropic conformation of polymer chains starts to be recovered to the uniform random conformation.

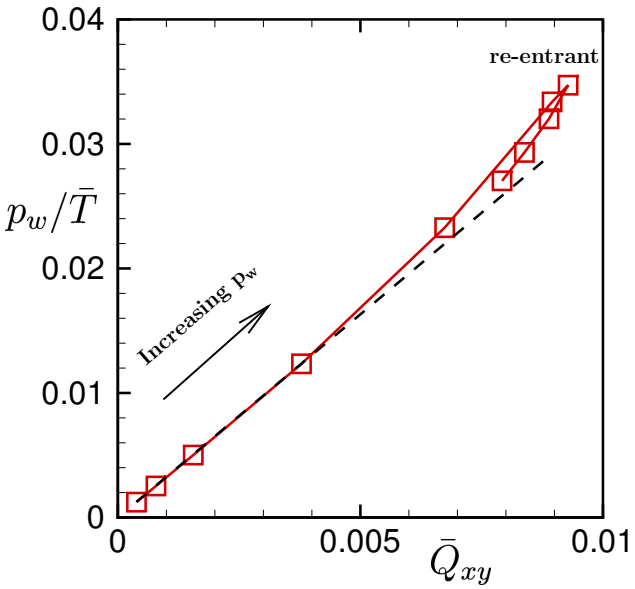

Figure 6. The stress–optical relation $p_w/\bar{T}$ vs. $\bar{Q}_{xy}$. The drive force p_w increases in the direction of the arrow. The re-entrant transition of the linear stress–optical relation is observed at large gross shear rates.

Figure 6 shows the stress–optical relation for the present problem. When the drive force p_w is small, the bond orientation $\bar{Q}_{xy}$ is linearly proportional to the drive force p_w, while the temperature is almost constant. Thus, a linear stress–optical relation is observed for $\bar{Q}_{xy} < 0.005$. As the drive force p_w increases, the results deviate from the linear relation.

However, surprisingly, the re-entrant transition of the linear stress–optical relation is observed at large drive force, where the temperature $\bar{T}$ rapidly increases and the bond orientations are recovered to be uniform and random. We note that the re-entrant transition of the linear stress–optical relation was also observed in the previous study for short polymer chains. These results confirm the robustness of the linear stress–optical relation of the polymeric liquid.

4.3. Time Evolution

Figure 7 shows the time evolutions of local velocities v_x, temperatures T, shear stresses p_{xy}, and bond orientations Q_{xy} at different positions for the drive force $p_w = 0.01$. It can be seen that the local shear stresses and bond orientations start to increase in the order of upper to lower positions because

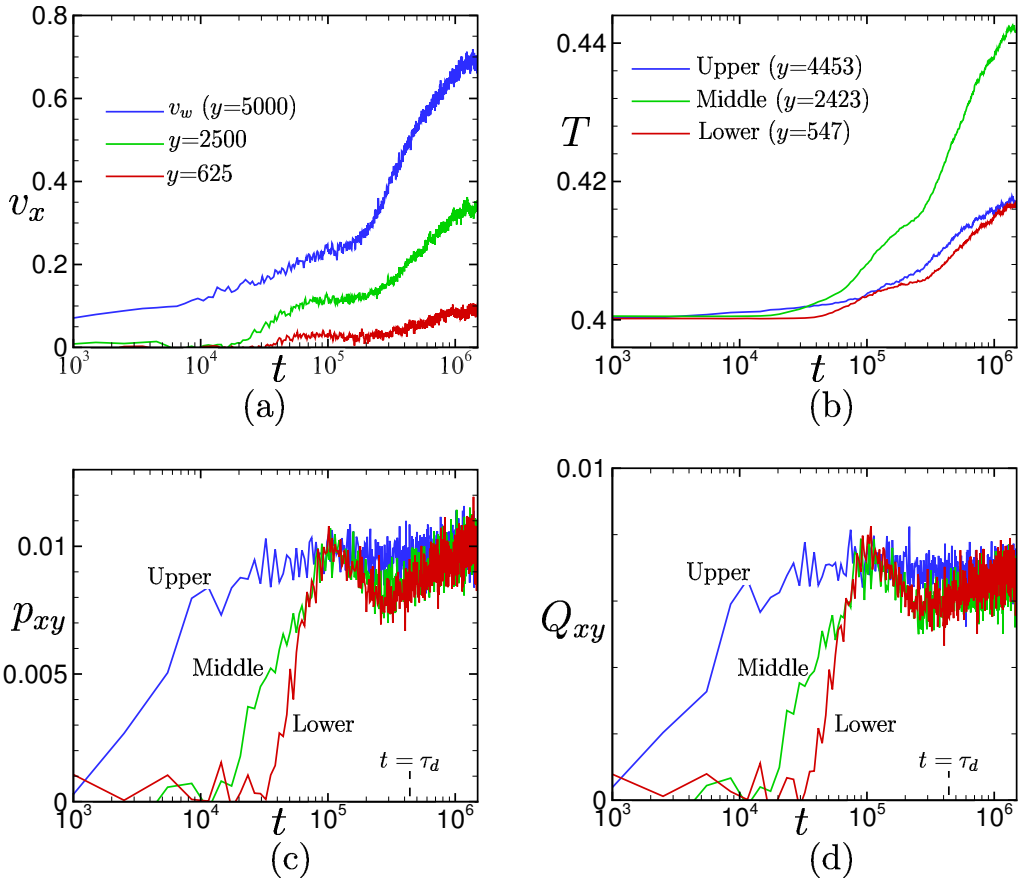

Figure 7. Time evolutions of (**a**) local velocity, (**b**) temperature, (**c**) shear stress, and (**d**) bond orientation for the drive force $p_w = 0.01$. The upper-wall velocity v_w and local velocities at y = 2500 and 625 are shown in (a). The local temperatures, local shear stresses, and local bond orientations at the upper (y = 4453), middle (y = 2423), and lower (y = 547) regions between the walls are shown in (b), (c), and (d), respectively. The vertical dashed line on the horizontal axis shows the disengagement time of entangled polymer chains in the quiescent state.

Preprints (www.preprints.org) | NOT PEER-REVIEWED | Posted: 8 November 2018 doi:10.20944/preprints201811.0223.v1

Peer-reviewed version available at Polymers 2019, 11, 131; doi:10.3390/polym11010131

the momentum is conducted from upper to lower positions. The shear stress and bond orientation increase rapidly and have local maxima at $t \sim 10^5$.

Yielding behaviors are clearly observed in the local shear stresses and bond orientations in $10^5 \lesssim t \lesssim \tau_d$. After the yielding, the velocity and temperature increase rapidly while the shear stress and bond orientation only vary slightly. It should be noted that the behaviors of the shear stress and bond orientation are quite similar to each other at each local position.

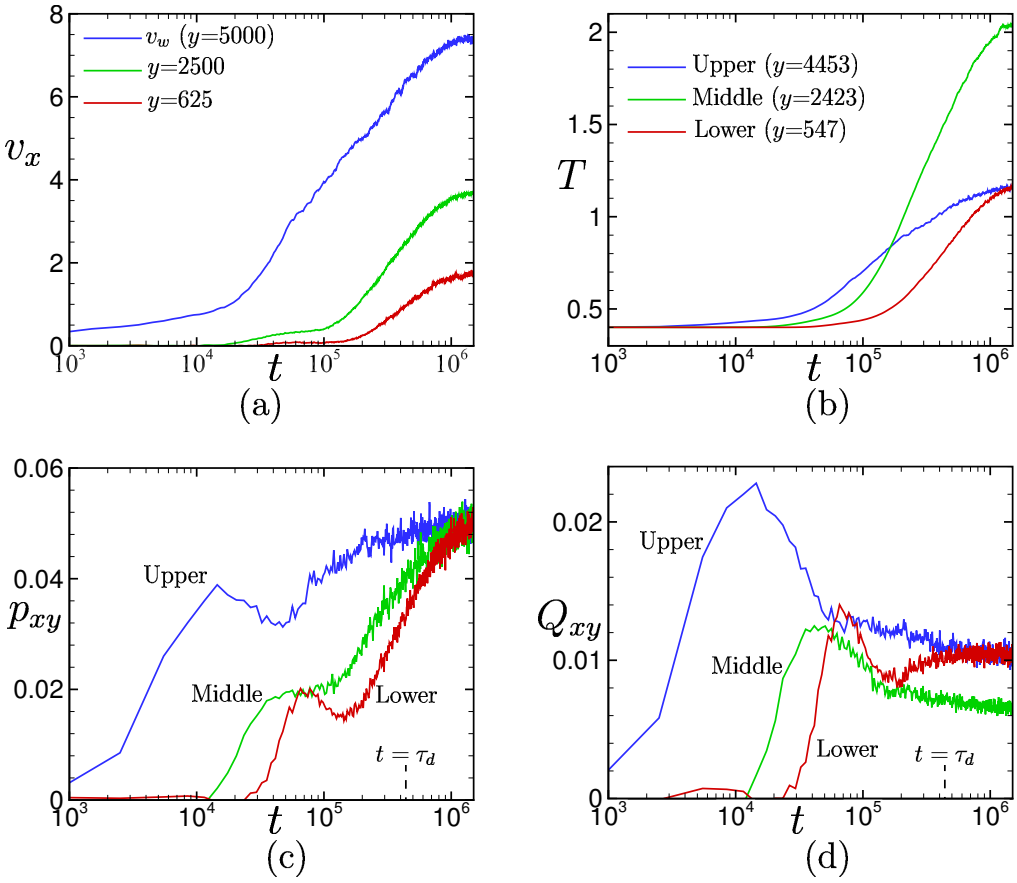

Figure 8. Time evolutions of (**a**) local velocity, (**b**) temperature, (**c**) shear stress, and (**d**) bond orientation for the drive force $p_w = 0.05$. See also the caption in Figure 7.

Figure 8 shows the time evolutions of local velocities, temperatures, shear stresses, and bond orientations for the drive force $p_w = 0.05$. Remarkable yielding behaviors are observed in the shear stress and bond orientation at the upper and lower positions (i.e., near the walls), where the local shear rates are very large (see also Figure 4). The local maxima are reached in the order of upper to lower positions, and the times to reach the local maxima are shorter than those in the case $p_w = 0.01$ (see Figure 7).

After the yielding, the velocity and temperature start to increase rapidly. This feature is also seen in Figure 7. However, the yielding behaviors of the shear stress and bond orientation are quite different from each other. The local shear stresses increase even after the yielding, and converge to the uniform value $p_{xy} = p_w$ while the local bond orientation decrease at the upper and middle positions but increase at the lower position.

The increase of shear stress after the yielding is highly correlated to the increase of temperature. This can be seen in Figure 9, where the time evolutions of the local shear stress divided by the local temperature p_{xy}/T are shown. Surprisingly, it can be seen in comparison with Figure 8d that the time evolutions of p_{xy}/T are similar to those of the bond orientations Q_{xy} at each position.

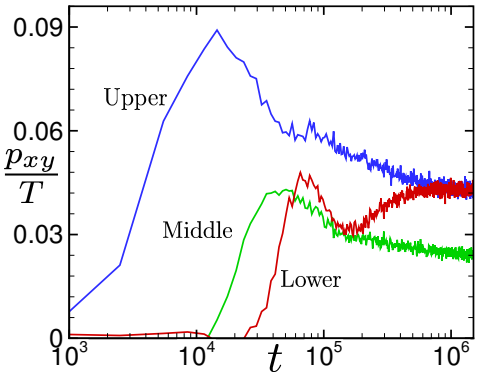

Figure 9. Time evolution of the local shear stress (shown in Figure 8c)) divided by the local temperature (shown in Figure 8b), p_{xy}/T for $p_w = 0.05$.

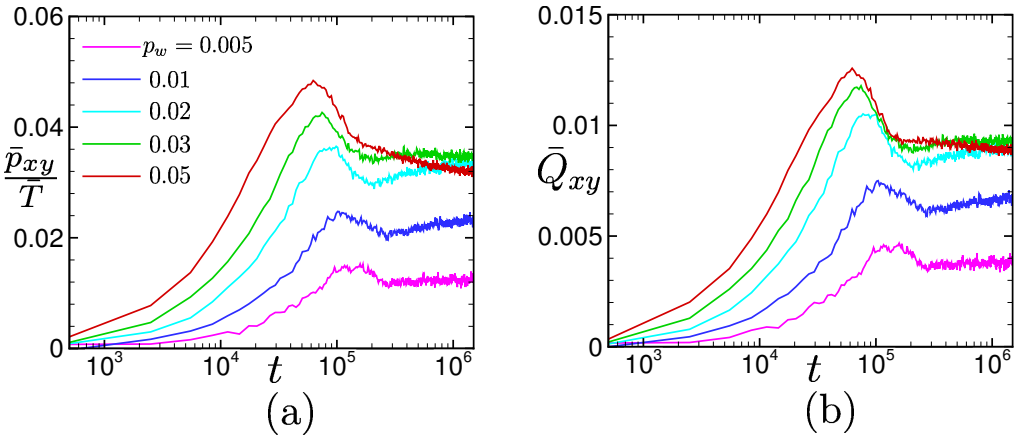

Figure 10. (**a**) Time evolutions of the spatial averages of the local shear stresses divided by the temperatures $\bar{p}_{xy}/\bar{T}$ and (**b**) the spatial averages of the local bond orientations $\bar{Q}_{xy}$ for different drive forces p_w.

Figure 10 shows the relations between $\bar{p}_{xy}/\bar{T}$ and $\bar{Q}_{xy}$, where the spatial averages are considered, for different drive forces p_w. It can be seen that for a small drive force (i.e., $p_w = 0.01$), both behaviors are almost synchronous. Even for large drive forces, the behaviors are similar to each other. These facts demonstrate that the linear stress–optical relation shown in Figure 6 approximately holds even locally and instantaneously at the hydrodynamic level.

5. Summary

We investigate the thermal lubrication of an entangled polymeric liquid in wall-driven shear flows between parallel plates by using the SMD method. The model polymeric liquid shows the characteristic behaviors of entangled polymer chains in the relaxation dynamics. That is, the transient behavior from the Rouse dynamics to the reptation dynamics is clearly observed in the stress relaxation function, as can be seen in Figure 2.

In the lubrication system, the temperature of the polymeric liquid increases in the middle of the channel due to viscous heating. The spatial profiles of other macroscopic quantities become also heterogeneous. The viscous heating becomes rapidly significant once the drive force exceeds a certain threshold value (i.e., $p_w \gtrsim 0.02$), as can be seen in Figure 4.

The gross rheological properties are also affected by the viscous heating. As can be seen in Figure 5a, the shear viscosity shows shear thinning behavior in the weak viscous-heating regime, while in the strong viscous-heating regime, it shows a weak viscous thickening behavior related to the rapid temperature rise. This behavior is quite different from that observed in the previous study, where a supercooled polymeric liquid composed of short chains was considered. In the previous study, the shear thinning behavior was further enhanced when the temperature rapidly increased in the strong viscous-heating regime. The physical mechanism for the qualitative different behaviors is not addressed in this paper.

Another remarkable observation is the transitional behavior of the conformational dynamics of polymer chains shown in Figure 5b. The transition is also triggered by the viscous heating. In the weak viscous-heating regime, the conformation of polymer chains is dominated by the local shear flow, so that the anisotropy of the bond orientation grows as the drive force increases. Surprisingly, in the strong viscous-heating regime, the conformation dynamics is dominated by the thermal agitation of polymer chains rather than the local flow field, so that the bond orientation tensor recovers the uniform random structure as the drive force increases, even though the local shear flow is further enhanced.

This counter-intuitive transitional behavior produces an interesting re-entrant transition in the stress–optical relation shown in Figure 6. The linear stress–optical relation shown in Figure 6 also approximately holds even locally and instantaneously at the hydrodynamic level. The robustness of the linear stress–optical relation can be observed in Figures 7–10.

The physical mechanism of the viscous-heating-induced transitional behavior in the entangled polymeric liquids will be addressed in detail in future studies.

Acknowledgments: This study was financially supported byJSPS KAKENHI Grant Number 16K17554 and 17H01083.

References

1. R. B. Bird, R. C. Armstrong, and O. Hassager, *Dynamics of polymeric liquids* Vol. 1; John Wiley and Sons, New York, 1987.
2. M. Laso and H. C. Öttinger, "Calculation of viscoelastic flow using molecular models: the CONNFFESSIT approach", *J. Non-Newtonian Fluid Mech.* **1993**, *47*, 1-20.
3. K. Feigl, M. Laso, and H. C. Öttinger, "CONNFFESSIT approach for solving a two-dimensional viscoelastic fluid problem", *Macromolecules* **1995**, *26*, 3261-3274.
4. M. Laso, M. Picasso, H. C. Öttinger, "2-D time-dependent viscoelastic flow calculations using CONNFFESSIT", *AIChE J.* **1997**, *43*, 877.

5. M. Dressler, B. J. Edwards, Öttinger, "Macroscopic thermodynamics of flowing polymeric liquids", *Rheol. Acta* **1999**, *38*, 117-136.
6. W. E and B. Engquist, "The heterogeneous multi-scale methods", *Comm. Math. Sci.* **2003**, *1*, 87-132.
7. W. Ren and W. E, "Heterogeneous multiscale method for the modeling of complex fluids and micro-fluidics", *J. Compt. Phys.* **2005**, *204*, 1-26.
8. M. M̈uller and K. C. Daoulas, "Speeding Up Intrinsically Slow Collective Processes in Particle Simulations by Concurrent Coupling to a Continuum Description", *Phys. Rev. Lett.* **2011**, *107*, 227801.
9. M. K. Borg, D. A. Lockerby, J. M. Reese, "A multiscale method for micro/nano flows of high aspect ratio", *J. Compt. Phys.* **2013**, *233*, 400-413.
10. I. G. Kevrekidis, C. W. Gear, J. M. Hyman, P. G. Kevrekidis, O. Runborg, and C. Theodoropoulos, "Equation-free, coarse-grained multiscale computation: enabling microscopic simulations to perform system-level analysis", *Comm. Math. Sci.* **2003**, *1*, 715.
11. I. G. Kevrekidis and G. Samaey, "Equation-free multiscale computation: algorithms and applications", *Annu. Rev. Phys. Chem.* **2009**, *60*, 321.
12. S. De, J. Fish, M. S. Shephard, P. Keblinski, and S. K. Kumar, "Multiscale modeling of polymer rheology", *Phys. Rev. E* **2006**, *74*, 030801(R).
13. S. De, "Computational study of the propagation of the longitudinal velocity in a polymer melt contained within a cylinder using a scale-bridging method", *Phys. Rev. E* **2013**, *88*, 052311.
14. T. Murashima and T. Taniguchi, "Multiscale Lagrangian Fluid Dynamics Simulation for Polymeric Fluid" *J. Polym. Sci. B* **2010**, *48*, 886.
15. T. Murashima and T. Taniguchi, "Multiscale Simulation of History Dependent Flow in Polymer Melt", *Europhys. Lett.* **2011**, *96*, 18002.
16. T. Murashima and T. Taniguchi, "Multiscale Simulation of History Dependent Flow in Polymer Melt", *J. Phys. Soc. Jpn.* **2012**, *81*, SA013.
17. M. J. Zimoń, R. Prosser, D.R/ Emerson, M. K. Borg, D. J. Baray, L. Grinberg, J. M. Reese, "An evalutation of noise reduction algorithms for particle-based fluid simulations in multi-scale applications", *J. Comput. Phys.* **2016**, *325*, 380-394.
18. S. Yasuda and R. Yamamoto, "A model for hybrid simulation of molecular dynamics and computational fluid dynamics", *Phys. Fluids* **2008**, *20*, 113101.
19. S. Yasuda and R. Yamamoto, "Rheological properties of polymer melt between rapidly oscillating plates: an application of multiscale modeling", *Europhys. Lett.* **2009**, *86*, 18002.
20. S. Yasuda and R. Yamamoto, "Multiscale modeling and simulation for polymer melt flows between parallel plates", *Phys. Rev. E* **2010**, *81*, 036308.
21. S. Yasuda and R. Yamamoto, "Dynamic rheology of a supercooled polymer melt in nonuniform oscillating flows between rapidly oscillating plates", *Phys. Rev. E* **2011**, *84*, 031501.
22. T. Murashima, S. Yasuda, T. Taniguchi, and R. Yamamoto, "Multiscale modeling for polymeric flow: particle-fluid bridging scale methods", *J. Phys. Soc. Jpn.* **2013**, *82*, 012001.
23. S. Yasuda and R. Yamamoto, "Synchronized molecular-dynamics simulation via macroscopic heat and momentum transfer", *Phys. Rev. X* **2014**, *4*, 041011.
24. S. Yasuda and R. Yamamoto, "Multiscale simulation for thermo–hydrodynamic lubrication of a polymeric liquid between parallel plate", *Mol. Sim.* **2015**, *41*, 1002-1005.
25. S. Yasuda and R. Yamamoto, "Synchronized molecular-ydnamics simulation for the thermal lubrication of a polymeric liquid between parallel plates", *Compt. Fluids* **2016**, *124*, 185-189.
26. M. Doi and S. F. Edwards, *The Theory of Polymer Dynamics* (Clarendon, Oxford, 1986).
27. K. Kremer and G. S. Grest, "Dynamics of entabgled linear polymer melts: A molecular-dynamics simulation," *J. Chem. Phys.* **1990**, *92*, 5057.
28. R. Yamamoto and A. Onuki, "Dynamics and rheology of a supercooled polymer melt in shear flow," *J. Chem. Phys.* **2002**, *117*, 2359.
29. R. Yamamoto and A. Onuki, "Entanglements in quiescent and sheared polymer melts", *Phys. Rev. E* **2004**, *70*, 041801.
30. M. P. Allen and D. J. Tildesley, *Computer Simulation of Liquids*; Oxford University Press, New York, 1989.
31. D. J. Evans and G. Morris, *Statistical mechanics of nonequilibrium liquids*; Cambridge university press, New York, 2008.